

LA-UR-23-33524

Accepted Manuscript

An exploration of anomalous electrical noise in shocked cyclotrimethylenetrinitramine (RDX)-based explosives

Burns, Malcolm John

Hopp, Bethany Ann Chidester

Provided by the author(s) and the Los Alamos National Laboratory (2024-09-30).

To be published in: Journal of Applied Physics

DOI to publisher's version: 10.1063/5.0191271

Permalink to record:

<https://permalink.lanl.gov/object/view?what=info:lanl-repo/lareport/LA-UR-23-33524>



Los Alamos National Laboratory, an affirmative action/equal opportunity employer, is operated by Triad National Security, LLC for the National Nuclear Security Administration of U.S. Department of Energy under contract 89233218CNA000001. By approving this article, the publisher recognizes that the U.S. Government retains nonexclusive, royalty-free license to publish or reproduce the published form of this contribution, or to allow others to do so, for U.S. Government purposes. Los Alamos National Laboratory requests that the publisher identify this article as work performed under the auspices of the U.S. Department of Energy. Los Alamos National Laboratory strongly supports academic freedom and a researcher's right to publish; as an institution, however, the Laboratory does not endorse the viewpoint of a publication or guarantee its technical correctness.

RESEARCH ARTICLE | APRIL 24 2024

An exploration of anomalous electrical noise in shocked cyclotrimethylenetrinitramine (RDX)-based explosives

M. J. Burns ; B. A. Chidester 



J. Appl. Phys. 135, 165903 (2024)

<https://doi.org/10.1063/5.0191271>



Articles You May Be Interested In

Influence of Al content and surrounding medium on the energy output of cyclotrimethylenetrinitramine (RDX)/Al/wax explosives

J. Appl. Phys. (February 2021)

Density functional theory calculations of anisotropic constitutive relationships in alpha-cyclotrimethylenetrinitramine

J. Appl. Phys. (December 2008)

Simulating thermal explosion of cyclotrimethylenetrinitramine-based explosives: Model comparison with experiment

J. Appl. Phys. (March 2005)

30 September 2024 16:28:38

Nanotechnology & Materials Science


Optics & Photonics

Impedance Analysis

Scanning Probe Microscopy


Sensors

Failure Analysis & Semiconductors



Unlock the Full Spectrum.
From DC to 8.5 GHz.
Your Application. Measured.

[Find out more](#)



An exploration of anomalous electrical noise in shocked cyclotrimethylenetrinitramine (RDX)-based explosives

Cite as: J. Appl. Phys. **135**, 165903 (2024); doi: [10.1063/5.0191271](https://doi.org/10.1063/5.0191271)

Submitted: 12 December 2023 · Accepted: 9 February 2024 ·

Published Online: 24 April 2024



View Online



Export Citation



CrossMark

M. J. Burns^{a)}  and B. A. Chidester 

AFFILIATIONS

Los Alamos National Laboratory, P.O. Box 1663, Los Alamos, New Mexico 87545, USA

^{a)}Author to whom correspondence should be addressed: malcolm.burns@awe.co.uk

ABSTRACT

Gas gun shock experiments on cyclotrimethylenetrinitramine (RDX)-based explosive compositions that employ embedded gauge particle velocity tracers have noted a significant amount of electrical noise when compared to other explosive formulations. This paper reexamines previously published embedded gauge data on Cyclotols (60–80 wt. % RDX) to quantify the electromagnetic behavior of these materials. The primary observation is a fourfold increase in the electrical noise when Cyclotols are shocked above 4.22 ± 0.08 GPa. Electromagnetic gauge noise is also observed within particle velocity traces in reactive growth and off-Hugoniot shocks, although at higher pressures than the direct shock case, suggesting a temperature- or kinetically dependent transition. In all cases, the electrical noise disappears upon detonation. By comparing with the static high-pressure phase diagram of RDX, we interpret this change in electromagnetic behavior to be a change in the RDX crystal structure to a piezoelectric phase, although it is uncertain whether the γ or ϵ phase is responsible for the observed behavior.

© 2024 Author(s). All article content, except where otherwise noted, is licensed under a Creative Commons Attribution-NonCommercial-NoDerivs 4.0 International (CC BY-NC-ND) license (<https://creativecommons.org/licenses/by-nc-nd/4.0/>). <https://doi.org/10.1063/5.0191271>

I. INTRODUCTION

Cyclotrimethylenetrinitramine (RDX) is a high explosive crystal (HE) that is commonly used in explosive formulations and monopropellants. As a secondary explosive, RDX is relatively safe and inexpensive to manufacture and yields a high power output, making it an excellent candidate in explosive fabrication. It is also easy to machine, mold, and shape. Since its discovery in the 1890s, followed by increasing production during World War II, it has been the subject of many investigations in terms of its bulk explosive properties and also its crystallographic nature. Recent studies on the effects of the composition of RDX and TNT (2,4,6-trinitrotoluene) blends (Cyclotols) have resulted in a better understanding of these mixtures in terms of detonation performance¹ and the effects of shock loading.^{2–7}

Shock-induced detonation behavior in HEs is often determined in gas gun facilities with a combination of optical diagnostics, such as the Velocimetry System for Any Reflector (VISAR) and Photon Doppler Velocimetry (PDV); electrical diagnostics such as Manganin gauges and PolyVinylidene Fluoride (PVDF) gauges; and embedded electromagnetic particle velocity (EPV) gauges to track shock and

particle velocities in the sample. A common observation in the EPV gauge data of RDX-based explosives is distinct electrical noise that is not observed in the complementary optical or electrical data. For example, the EPV data presented in Fig. 1, reproduced from Burns *et al.*,⁴ show the particle velocities in a Composition B target with an input pressure of 5.12 GPa. For reference, the following discussion will point the reader to actual gas gun experimental data using the shot number, where 1s-xxxx and 2s-xxxx refer to the single and two-stage gas guns, respectively. The wave profiles are noisy until the material transitions to detonation at a depth of ~ 4.43 mm (teal curve, Fig. 1). Dattelbaum *et al.* saw similarly high electrical noise in embedded gauge data on Composition B3 that was not reflected in the companion VISAR data.² Importantly, the electrical noise of this magnitude is not observed in similar experiments with other explosives.

In all of these cases, the electrical noise has been interpreted as piezoelectric charge buildup in the RDX crystals.^{2–5} At ambient pressure, RDX has been shown to be “tensorially piezoelectric,” where the piezoelectric coefficient depends on the force applied to the crystal and is ~ 10 – 100 times smaller than that of PETN (pentaerythritol tetranitrate), a truly piezoelectric explosive crystal.⁸

30 September 2024, 16:28:38

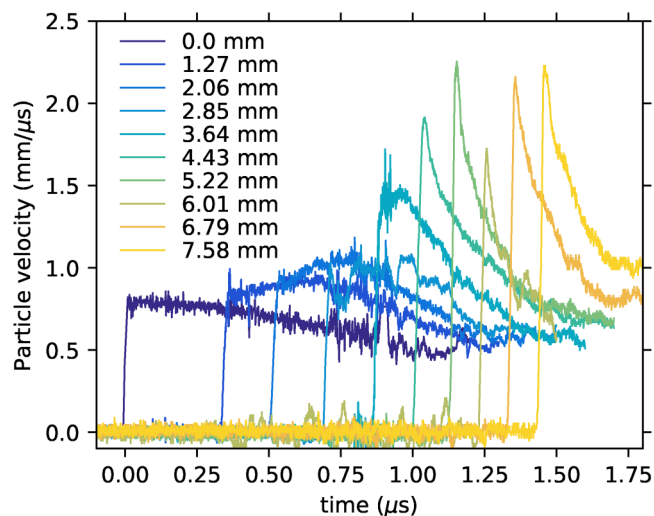


FIG. 1. Shot 2s-963 on Composition B. Curves represent the EPV gauges embedded within the sample at different depths (measured in millimeters). The initial shock pressure (black curve) was 5.12 GPa. Detonation, indicated by the triangular detonation wave shape, occurs around 4.43 mm (teal curve).

However, RDX has a complex high-pressure, high-temperature phase diagram, and it is likely to undergo crystallographic phase transitions on the runup to detonation.^{9–13} The mechano-electric properties of high-pressure phases of RDX are not known, but given the known crystal structures, true piezoelectric character is possible. Piezoelectricity in HE crystals may affect the process of detonation, so its presence and amplitude must be quantified for inclusion in models of detonation. We re-examined the embedded electromagnetic gauge data from previous studies to further explore the relationship of electromagnetic noise in embedded gauge experiments on RDX-based explosives at a range of pressures. We discuss our results in relation to the RDX phase diagram.

II. EXPERIMENTAL DETAILS

All of the experiments discussed in this paper were carried out at the gas gun facility in Chamber 9 located in Technical Area 40 at the Los Alamos National Laboratory (LANL). The single- and two-stage gas guns have bore diameters of 72 and 50 mm, respectively, leading to maximum one-dimensional shock loading depths of 36 and 25 mm. The gas guns were used to launch non-metallic impactors (typically sapphire or Kel-F) in the velocity range of 0.2–3.1 km/s. The target samples, which typically consist of a split cylindrical wedge of Cyclotol, were embedded with EPV gauges to track particle velocity through the target. This is the standard technique, which has been utilized at LANL since the mid-1980s; a good description of the technique can be found in the publication by Sheffield *et al.*,¹⁴ and several papers discussing the application of the method can be found in Refs. 15–17.

Figure 2 shows the photo of the embedded gauges with the individual gauge elements and the three tracker gauges as annotated. The gauge package consists of nine particle velocity gauges

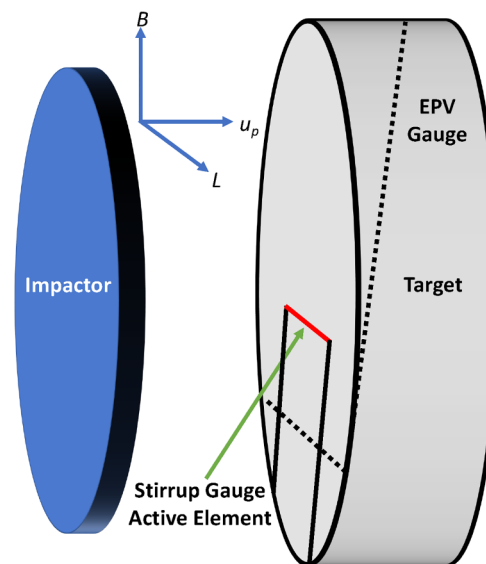
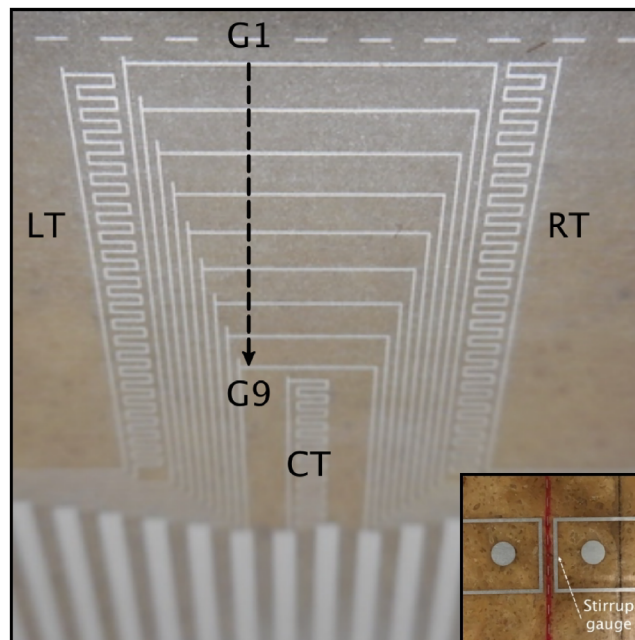


FIG. 2. Top: photograph of the embedded particle velocity gauge showing the positions of gauge one (G1) to gauge nine (G9), along with the left (LT), right (RT), and central tracker (CT) gauges. The inset shows the front surface stirrup gauge—of which only the right gauge was used. Bottom: schematic of experimental setup showing the impactor and the split cylindrical explosive target with embedded particle velocity gauges and stirrup gauge. Also shown are the relative directions of the magnetic field (B), gauge length (L), and particle velocity (u_p) vectors.

nested one inside the other with the active element of the gauge being the horizontal portion. Each gauge consists of a thin ($\approx 5\mu\text{m}$) aluminum element sandwiched between insulating sheets of fluorinated ethylene propylene (FEP) Teflon. When the shock drives the

30 September 2024, 16:28:38

active (horizontal) part of the gauge (at particle velocity u_p) through an applied magnetic field (B), it produces the net voltage (v) according to

$$v = BLu_p. \quad (1)$$

Here, the length (L) of the active elements ranges from ~ 5 to 15 mm. Typically, these gauges are placed at an angle of 30° , resulting in a depth spacing of ~ 1 mm in the direction of the shock and covering a depth in the region of 1–10 mm. Surrounding the nested particle velocity gauges are the three shock tracker gauges. These ladder-like structures provide a change in the polarity of the voltage signal as the shock transits between each rung in the ladder. This provides ~ 130 individual measurements of the shock position as a function of time.

The gauges are glued onto the bottom wedge with careful alignment to the impact plane. The top wedge is then glued in place with a glue bond thickness of less than $10 \mu\text{m}$. The complete gauge layer is typically less than $50 \mu\text{m}$. The front surface of the target is machined flat, and a single element EPV *stirrup* gauge is glued onto the impact surface.

III. OBSERVATIONS ON SHOCK INITIATION DATA

This section summarizes a number of different shock initiation regimes presented in the literature describing qualitative observations of electrical noise in particle wave velocity profiles. One of the benefits of the embedded electro-magnetic gauges is that the

closely spaced, independent gauge elements all act as antennas in which one can detect peripheral electrical signals.

A. Distinct change in electrical behavior at ~ 4.2 GPa

To quantify the electrical noise amplitude in EPV gauge data with RDX-based explosives, we analyzed the frequency content of several wave profiles using an adaptation of the spectrogram function of ObsPy.¹⁸ An example of that analysis is given for stirrup gauge data in Fig. 3 for two identical Cyclotol targets at different input pressures. In typical gauge data, the measured particle velocity is zero until the shock or detonation wave arrives at the physical gauge, at which point the gauge records a jump in voltage (see Fig. 1, for example). The stirrup gauge is at the target surface (0 mm depth, Fig. 2), so it records the initial shock state of the sample. In our analysis of the gauge noise (Fig. 3), the large amplitude jump in signal at the shock wave arrival was filtered out of the data with a high-pass filter at 50 MHz (blue curves), with the original data in black. In the panels to the right, the spectrograms of filtered data are plotted as frequency as a function of time where the colorbar represents the power density (essentially the amplitude) of the noise.

A large range of experiments have been carried out by Burns *et al.*^{4,5} on two Cyclotol formulations, one with 75% RDX and 25% TNT by weight and the other a UK formulation of Composition B. Figure 3 illustrates a common scenario observed in those experiments. The top panels in the figure show the stirrup gauge trace from Shot 1s-1627, which had an input pressure of 3.36 GPa. The data are relatively clean, and the power spectrum on the right shows no distinct features apart from one wiggle from the

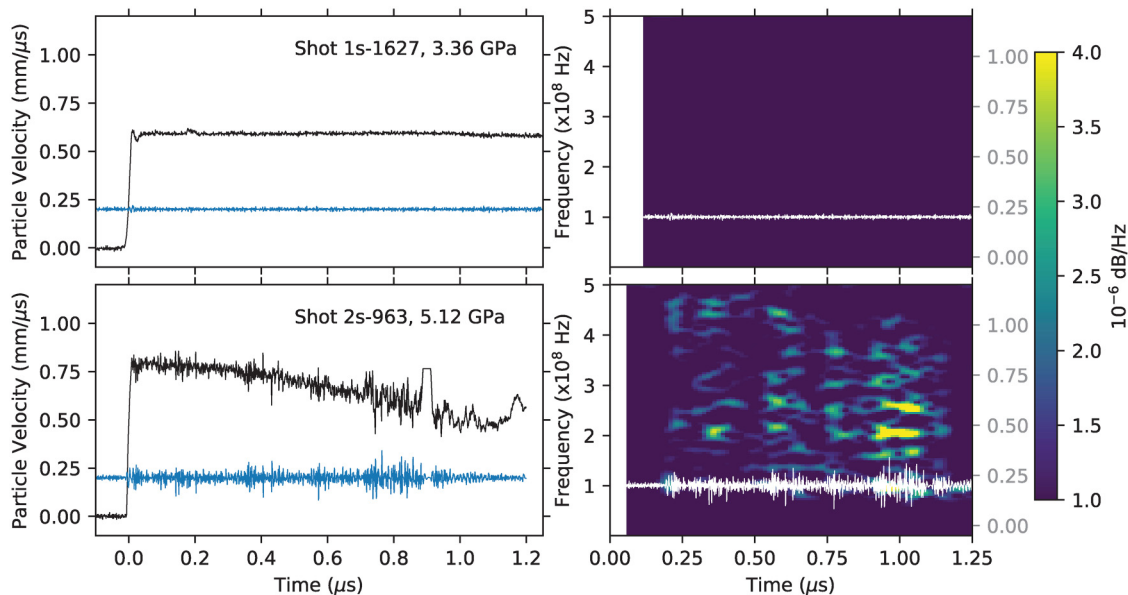


FIG. 3. Frequency analysis of the electrical noise in the stirrup gauges of two shots: 1s-1627 and 2s-963, at 3.36 and 5.12 GPa, respectively. Left panels show the original wave profiles in black. Blue curves are the wave profiles filtered to remove the jump in particle velocity at time = 0 s. Panels on the right show the spectrograms of the filtered data as a function of time, with noise amplitude demonstrated with the colorbar. White curves are the filtered wave profiles for reference, with the particle velocity axis to the right.

30 September 2024, 16:28:38

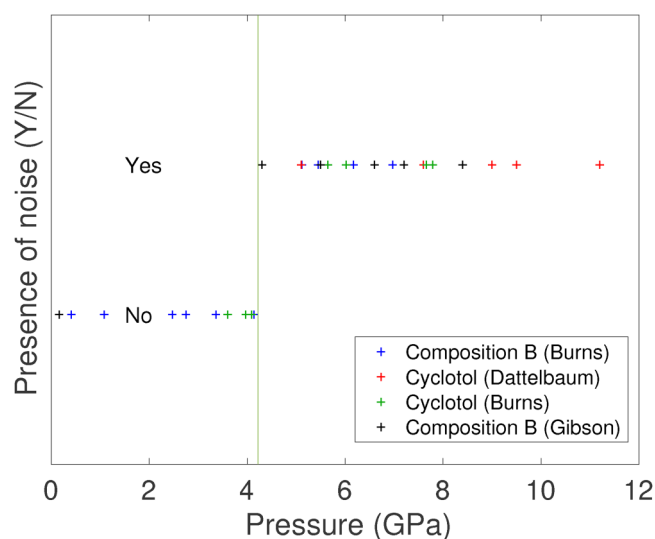


FIG. 4. Compilation of EPV gauge data showing a distinct change in the electrical noise content at 4.22 ± 0.08 GPa.

shock arrival. In contrast, the data from Shot 2s-963 with an input pressure of 5.12 GPa (bottom panels) are comparatively very noisy. The power spectrum on the right shows variable noise amplitude more than four times higher than the lower pressure example.

As mentioned above, the large amplitude noise in EPV gauge data has been attributed to possible piezoelectric charge buildup in the RDX crystals. However, not all of the electromagnetic gauge data collected could be qualified as “noisy.” We re-examined existing electromagnetic gauge data from many different gas gun experiments^{2–5} to determine whether the change in electrical signal occurs systematically at a distinct pressure. Figure 4 provides a simple “Yes/No” chart for these experiments, where relatively clean data are in the bottom row and noisy data are in the top row. Based on this analysis, it is clear that there is a distinct change in the data quality at 4.22 ± 0.08 GPa.

B. Results from reactive growth and off-Hugoniot experiments

An interesting test of this transition pressure is possible with reactive growth within HE targets, because the pressure in the system increases as the reaction proceeds toward detonation. In shot 1s-1627 (Fig. 5), the sample was initially shocked to 3.36 GPa, below the threshold pressure for noisy gauge data from Fig. 4. However, when the shock wave reaches Gauge 7 (around $1.9 \mu\text{s}$), the signal is suddenly significantly noisier (Fig. 5). Each electrical gauge embedded within the sample works like antenna, so the increase in noise registers on all of them at the same time. The noise in the gauge data lasts for around $0.4 \mu\text{s}$ and decreases suddenly when the sample reaches detonation (i.e., Gauge 9 in Fig. 5). From the known Hugoniot for this explosive, we estimate that the pressure at the shock front at Gauge 7 in this sample is 6.86 ± 0.05 GPa. This is well above the threshold pressure expected

for this transition based on the data presented above, suggesting that the transition is affected by either temperature or kinetics, or both, in a reactive growth scenario.

Another scenario is that of the double shock experiment presented in Fig. 6 (shot 1s-1653 on Cyclotol 75/25). In this target configuration, the sample is initially shocked to ~ 3 GPa and that shock wave is followed $0.75 \mu\text{s}$ later by a stronger shock at ~ 8 GPa. In this example, neither the input shock wave nor the following stronger shock leads to any induced electrical noise. However, as soon as the second shock catches the primary shock ($\sim 1.8 \mu\text{s}$, just after the shock wave hits Gauge 6), there is observable noise both behind the shock front, and also in the base line of the three gauges ahead of the shock at the point of coalescence. Given the results discussed in Sec. III A, one would expect the data to become noisy immediately as the second shock pushes the sample to ~ 8 GPa. Again, the delay in transition could be due to temperature and/or kinetics. Although the second shock is above the expected transition pressure of 4.22 GPa, it is interacting with pre-densified HE, which will reach lower temperatures than ambient-density HE compressed to the same pressure. This supports the hypothesis that the transition to a piezoelectric crystal is temperature dependent and/or kinetically inhibited. Interestingly, the wave profiles from this experiment are only noisy for $\sim 0.6 \mu\text{s}$, after which the signal quiets significantly even though the HE never turned over to detonation. In this case, the RDX crystals may have decomposed or transitioned to yet another solid phase.

C. Comparison to other HEs

To demonstrate “normal” EPV data from gas gun experiments at the LANL single and two-stage gas gun facilities, the analysis described above was carried out for Polymer Bonded Explosives (PBXs) and melt-cast explosives that do not contain RDX. A large survey was taken from explosives based on the following explosive crystals: HMX (also known as Octogen), TNT, and TATB (2,4,6-triamino-1,3,5-trinitrobenzene). Figure 7 shows a selection of those analyzed. In all cases, there was no evidence of any electrical noise other than the stochastic noise typically seen in these experiments. Figure 7 combines the simplified wave profiles from seven different experiments. In each case, the wave profile presented is the one recorded just before the turn over to detonation (~ 20 – 30 GPa), as this is typically the highest level of noise in an RDX-based experiment. The input pressures for these experiments ranged from ~ 2 to ~ 10 GPa; somewhat similar to that of the RDX-based experimentation discussed. The type of explosive crystal and estimated pressure at that position is also noted in the figure. The spectrogram to the right of Fig. 7 corresponds to shot TATB 1109 at 23.1 GPa. In this instance, the color bar is plotted on the same scale as those in Figs. 3 and 5. The amplitude of the noise for these HEs is concentrated at the lower end of the colorbar, similar to RDX-based explosives below 4.3 GPa. This suggests that the noise in the EPV gauge data is due to the RDX. Note that TNT cannot be the root cause of this electrical noise as TNT is also present in all Octol compositions. In the work of Dattelbaum² on the 81.6% HMX and 20.2% TNT Octol blend, the data were very clean and free of spurious electrical noise. As mentioned above, PETN is truly piezoelectric at ambient conditions, so it would be an ideal way to

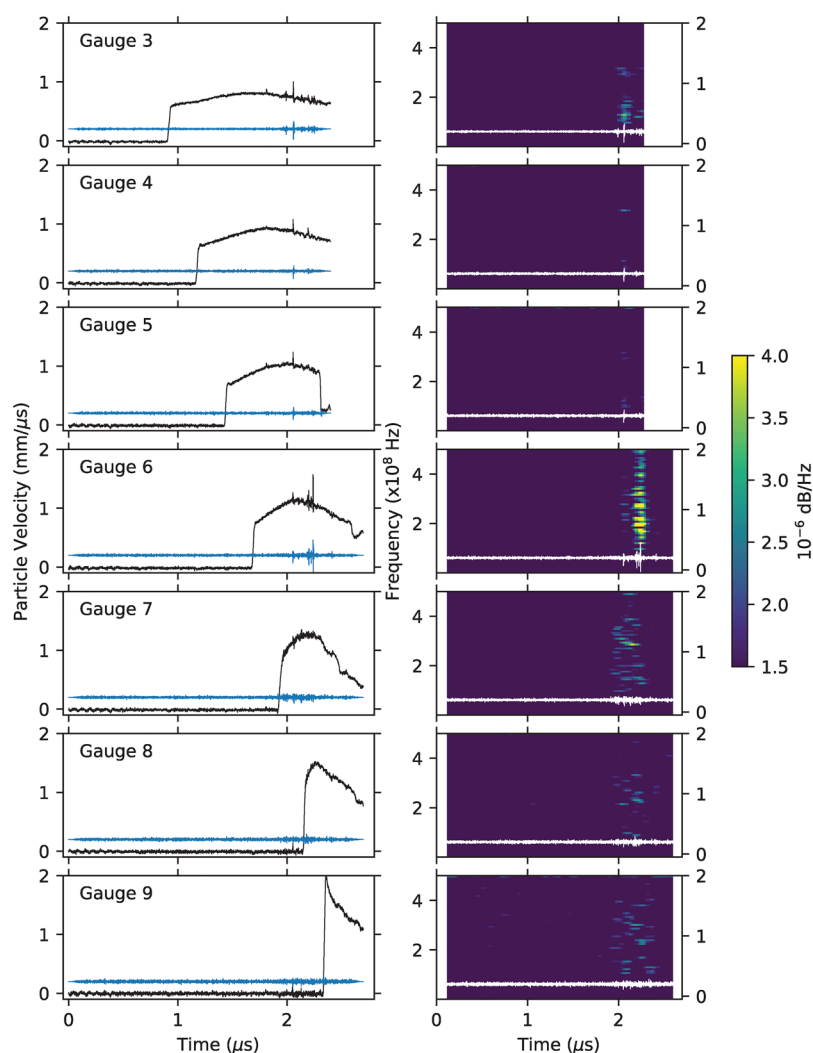


FIG. 5. Data from Shot 1s-1627 showing electrical gauge traces (left panels, black curves), filtered traces (left panels, blue curves), and spectrograms (right panels). The filtered traces are also provided in the right panels (right axes) as white curves for easy comparison.

study this phenomenon. However, PETN is so highly reactive that it is not typically studied with embedded EPV gauges.

D. The high P - T phase diagram of RDX

The sharp change in behavior at ~ 4.2 GPa (Fig. 4) suggests that the principal Hugoniot (i.e., the locus of end states realized in pure shock) of RDX traverses a crystallographic phase boundary at that pressure. Previous static high-pressure studies in a diamond anvil cell (DAC) have identified four crystalline phases of RDX below 10 GPa (see Fig. 8). The ambient-pressure, room-temperature phase (α -RDX) takes an orthorhombic crystal structure ($Pbca$, $Z=8$),¹⁹ and as mentioned above, is tensorially piezoelectric. Another phase, β -RDX, exists at ambient pressure and is synthesized by crystallization at high temperatures.²⁰ However, β -RDX is known to be very unstable and reverts to the α phase when in contact with α crystals,^{21–23} so it is likely not important to this process. At 3.8–4.1 GPa and 4 K to at least 380 K,^{9,24} α -RDX transforms

to γ -RDX, another orthorhombic crystal with space group $Pca2_1$ ($Z = 8$).²⁵ While this transition pressure is very similar to our observed change in behavior, there is another crystallographic phase of RDX, the ε phase (space group $Pca2_1$, $Z = 4$), which is known to exist between ~ 2 –6 GPa and high temperatures. The transition temperature for ε -RDX is uncertain; it has been observed as low as 380 K²⁴ and as high as 500 K at ~ 4 GPa.²⁶ As both γ - and ε -RDX take the space group $Pca2_1$, they are both non-centrosymmetric orthorhombic crystals (point group $mm2$) so they could both be piezoelectric in principle. *Note that temperature is incredibly difficult to measure under shock conditions and was not measured in any of the experiments described here.*

In shock configurations that are off the principal Hugoniot, including reactive growth (e.g., Fig. 5) or double shock scenarios (e.g., Fig. 6), the change in electrical behavior is at higher pressures than in the direct shock situation. This suggests that either the phase transition of interest is temperature dependent, favoring the ε phase, or that the phase transition is kinetically inhibited and

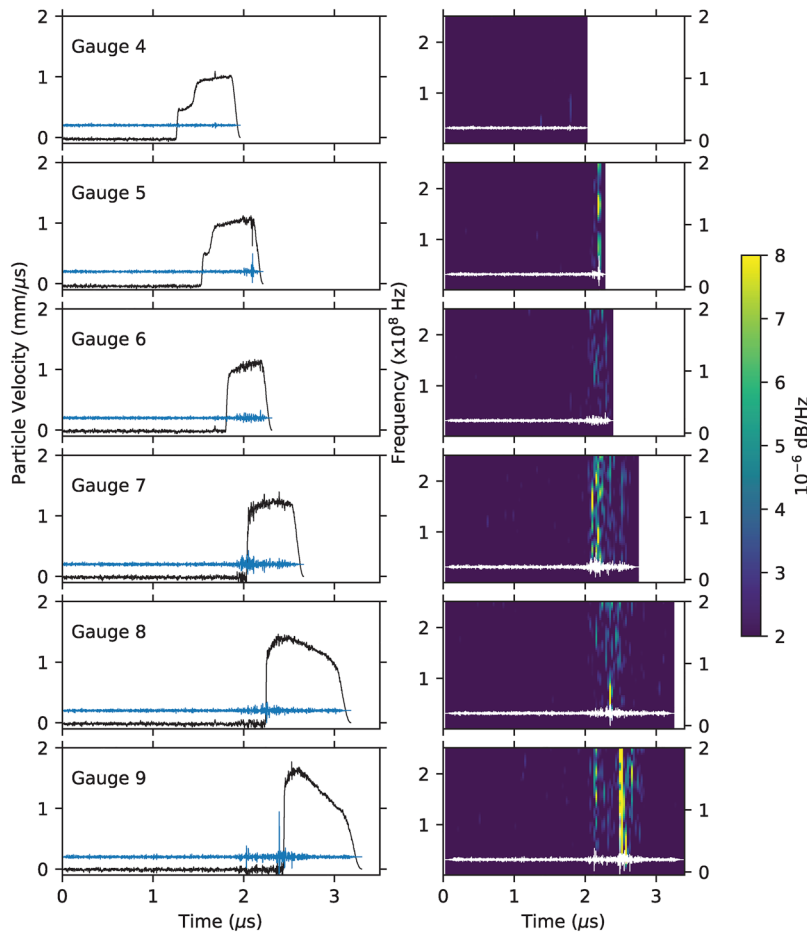


FIG. 6. Cyclotol 75/25 Shot1s-1653. Input pressures of 2.93 and 7.97 GPa.

30 September 2024, 16:28:38

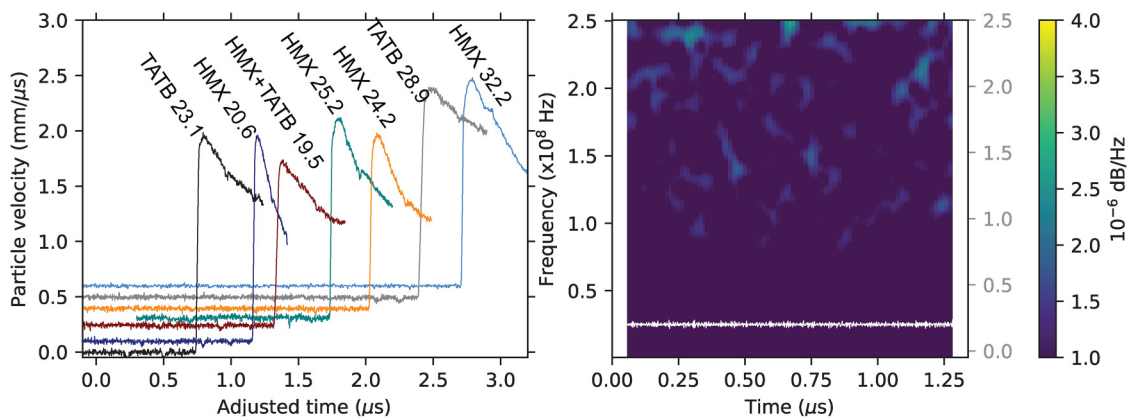


FIG. 7. Left: EPV data for different HE-based explosives just prior to detonation. The estimated pressure in GPa at the reaction front associated with each trace is noted. Right: Spectrograph for TATB (23.1 GPa, black curve at earliest time) plotted on the same power scale as the traces in Figs. 3 and 5.

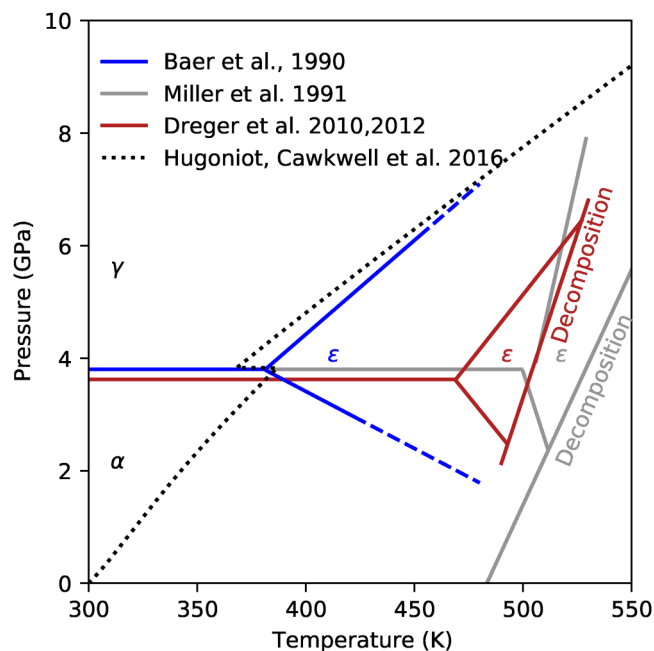


FIG. 8. The static high P - T phase diagram of RDX^{11,24,26,27} with the calculated shock Hugoniot.²⁸ Phase boundaries are approximate.

could be either the γ or ϵ phase. In the work of Patterson *et al.*,²⁹ single crystals of RDX were subjected to a ring-up shock to a peak pressure of 5.5 GPa. A ring-up experiment will also be at lower temperature than a shock on the principal Hugoniot, so it is analogous to the double shock experiment discussed in Sec. III B. Time-resolved Raman spectroscopy from that study determined that RDX undergoes a phase transition to the γ phase between 3.0 and 4.5 GPa. Whether that is true in pure shock loading is unclear. To further complicate the situation, given that both the γ and ϵ phases are non-centrosymmetric structures and so could both be piezoelectric, it is possible that either or both phases are contributing to electrical noise depending on the shock configuration.

Given the uncertainty in the high P - T phase diagram of RDX, and the unknown kinetic properties of this material, it is not clear which phase is responsible for the observed change in behavior. While this might seem trivial, understanding which phases are present at the leading edge of the detonation front and having good constraints on their properties are imperative for modeling detonation. Ultimately, since either phase may be present, depending on the temperature, and both phases could be piezoelectric, either or both phases could play a role in detonation. Future studies should work to constrain both the phase diagram and the structural behavior of RDX in shock experiments. Ideally, shock experiments would be undertaken to measure the piezoelectric response of RDX directly.

E. Other possible sources of electric noise

One possible source of electrical noise in this type of experimentation is in the breaking of gauge legs with shock progression.

This would have the effect of producing spurious electrical noise that would be observed on neighboring gauge elements as crosstalk. At this time, all gauges would measure an increased noise level. This noise is typically observed in these experiments and seen in all HE types. It is likely that we observe this noise in addition to the noise discussed in this paper. The one noticeable feature of the electrical noise in RDX-based explosives is its predictability.

Could it be possible that the insulating material in the projectile is subject to shock-induced electrical breakdown causing a perturbation in the magnetic field, and, therefore, the experimental data? While the effects of shock induced resistance breakdown have been observed in insulator materials subject to electrical potentials ranging from a few hundred volts³⁰ to tens of kilovolts,³¹ the effects of this are not observed in this type of experimentation. If it were observed, it would be ubiquitous in embedded gauge experimental data, and not only observed in a predictable manner as seen in this work. Perhaps any decrease in resistance is not sufficient to induce a change in the local magnetic field and, therefore, perturb the experimental data.

It is also possible that the noise discussed in this paper is a result of fracto-emission caused when the explosive crystals crack on shock loading. In the work of Sheffield *et al.*³² embedded gauges were used to study low pressure shock phenomenon in sugar (used as an inert simulant for HMX). It was apparent that the coarse sugar, when shock loaded resulted in intense noise in the particle velocity wave profiles. In his paper, Sheffield attributed this to possible fracto-emission in the sugar crystals. This effect has been studied in a variety of materials including RDX,³³ PETN,³⁴ and LifeSaver candy.³⁵ In these experiments, crystals of the order of a few millimeters were subject to compression and three point loading and both electron and positron emissions were observed with a channel electron multiplier positioned 1 cm from the sample. However, the emission was recorded over a timescale of hundreds of seconds, as opposed to the microsecond timescale of our shock experiments. It remains to be possible that this is what we are observing. Future experiments would be required to separate both the piezoelectric and fracto-emission processes to determine what we are observing in our shock to detonation experiments.

IV. CONCLUSIONS

This paper has reviewed the results of a range of shock initiation experiments carried out on RDX, HMX, TNT, and TATB based explosives. This investigation has found that the RDX-based explosives display a high degree of electrical noise in the embedded electromagnetic gauge experiment. This noise is attributed to shock-induced piezoelectricity, and it has been noted that this effect is only observed in the γ -phase (or possibly ϵ -phase) of the RDX crystals.

Comparison was made to similar shock initiation experiments on HMX, TNT, and TATB based explosives, where no electrical noise was present.

Additionally, experiments where the RDX-based explosives were shocked below the α - γ phase boundary show that as the shock progresses through the explosive sample, and the reactive growth pushed the pressure to the higher pressure states, the piezoelectric noise has been observed to switch on for several hundred nanoseconds, until the onset of detonation. The pressures at which

this occurs have been measured above that of the phase boundary, indicating that this observable is effected by phase change kinetics.

The observation of shock-induced piezoelectricity could have implications in the accurate modeling of the complex response of RDX-based explosives to shock stimuli. The interplay between electrical effects and shock sensitivity remain to be an interesting area of research in explosive science.

ACKNOWLEDGMENTS

B.A.C. was funded by a LANL Director's Postdoctoral Fellowship under LDRD Project No. 20210943PRD2. The authors would like to thank Dr. Chet Hopp for help with frequency noise analysis using ObsPy and Dana Dattelbaum for many fruitful discussions on this topic. This work was supported by the US Department of Energy through the Los Alamos National Laboratory. Los Alamos National Laboratory is operated by Triad National Security, LLC, for the National Nuclear Security Administration of U.S. Department of Energy (Contract No. 89233218CNA000001).

AUTHOR DECLARATIONS

Conflict of Interest

The authors have no conflicts to disclose.

Author Contributions

M. J. Burns: Conceptualization (lead); Data curation (equal); Formal analysis (equal); Writing – original draft (equal); Writing – review & editing (equal). **B. A. Chidester:** Data curation (equal); Formal analysis (equal); Writing – original draft (equal); Writing – review & editing (equal).

DATA AVAILABILITY

The data that support the findings of this study are available from the corresponding author upon reasonable request.

REFERENCES

- ¹T. A. Kuiper, E. K. Anderson, M. Short, and S. I. Jackson, "Detonation performance measurements of cyclotol 80/20," *AIP Conf. Proc.* **1793**(1), 030003 (2017).
- ²D. M. Dattelbaum, R. L. Gustavsen, M. J. Burns, L. L. Gibson, B. D. Bartram, A. Goodbody, and J. D. Jones, "Shock initiation sensitivities of cast TNT-based explosives: Cyclotol and Octol," in *Proceedings of the 16th International Detonation Symposium* (Office of Naval Research, 2018).
- ³L. L. Gibson, D. M. Dattelbaum, B. D. Bartram, S. A. Sheffield, R. L. Gustavsen, G. W. Brown, M. M. Sandstrom, A. M. Giambra, and C. A. Handley, "Shock initiation sensitivity and Hugoniot-based equation of state of composition B obtained using in situ electromagnetic gauging," *J. Phys.: Conf. Ser.* **500**(19), 192004 (2014).
- ⁴M. J. Burns, L. L. Gibson, J. D. Jones, A. B. Goodbody, D. M. Dattelbaum, and R. L. Gustavsen, "One dimensional shock initiation of hot isostatically pressed composition B," *AIP Conf. Proc.* **1979**(1), 150007 (2018).
- ⁵M. J. Burns, C. Chiquete, J. D. Jones, A. T. Houlton, L. L. Gibson, and B. D. Bartram, "Shock initiation of cyclotol (75/25) at both ambient temperature and 70 °C," *AIP Conf. Proc.* **2272**(1), 050006 (2020).
- ⁶K. S. Vandersall, F. Garcia, and C. M. Tarver, "Shock initiation experiments with ignition and growth modeling on low density composition B," *AIP Conf. Proc.* **1793**, 040015 (2017).
- ⁷P. A. Urtiew, K. S. Vandersall, C. M. Tarver, F. Garcia, and J. W. Forbes, "Shock initiation experiments and modeling of composition B and C-4," in *Thirteenth International Detonation Symposium* (Office of Naval Research, 2006), pp. 929–939.
- ⁸K. Raha and J. S. Chhabra, "Static charge development and impact sensitivity of high explosives," *J. Hazard. Mater.* **34**, 385–391 (1993).
- ⁹J. A. Ciezak and T. A. Jenkins, "The low-temperature high-pressure phase diagram of energetic materials: I. Hexahydro-1,3,5-trinitro-s-triazine," *Propellants, Explos., Pyrotech.* **33**(5), 390–395 (2008).
- ¹⁰Z. A. Dreger and Y. M. Gupta, "Phase diagram of hexahydro-1,3,5-trinitro-1,3,5-triazine crystals at high pressures and temperatures," *J. Phys. Chem. A* **114**(31), 8099–8105 (2010).
- ¹¹Z. A. Dreger, M. D. McCluskey, and Y. M. Gupta, "High pressure–high temperature decomposition of γ -cyclotrimethylene trinitramine," *J. Phys. Chem. A* **116**(39), 9680–9688 (2012).
- ¹²C. Gao, C. Zhang, Z. Sui, Y. Qu, R. Dai, Z. Wang, X. Zheng, and Z. Zhang, "Phase transition of RDX under high pressure up to 50 GPa," in *26th International Colloquium on the Dynamics of Explosions and Reactive Systems* (The Combustion Institute, 2017), p. 0902.
- ¹³C. Gao, X. Zhang, C. Zhang, Z. Sui, M. Hou, R. Dai, Z. Wang, X. Zheng, and Z. Zhang, "Effect of pressure gradient and new phases for 1,3,5-trinitrohexahydro-s-triazine (RDX) under high pressures," *Phys. Chem. Chem. Phys.* **20**, 14374–14383 (2018).
- ¹⁴S. A. Sheffield, R. L. Gustavsen, and R. R. Alcon, "In-situ magnetic gauging technique used at LANL-method and shock information obtained," *AIP Conf. Proc.* **505**(1), 1043–1048 (2000).
- ¹⁵M. J. Burns, R. L. Gustavsen, and B. D. Bartram, "One-dimensional plate impact experiments on the cyclotetramethylene tetranitramine (HMX) based explosive EDC32," *J. Appl. Phys.* **112**(6), 064910 (2012).
- ¹⁶R. L. Gustavsen, S. A. Sheffield, R. R. Alcon, J. W. Forbes, C. M. Tarver, and F. Garcia, "Embedded electromagnetic gauge measurements and modeling of shock initiation in the TATB based explosives LX17 and PBX 9502," *AIP Conf. Proc.* **620**(1), 1019–1022 (2002).
- ¹⁷R. L. Gustavsen, S. A. Sheffield, and R. R. Alcon, "Extended run distance measurements of shock initiation in PBX 9502," *AIP Conf. Proc.* **955**(1), 915–918 (2007).
- ¹⁸L. Krischer, T. Megies, R. Barsch, M. Beyreuther, T. Lecocq, C. Caudron, and J. Wassermann, "ObsPy: A bridge for seismology into the scientific python ecosystem," *Comput. Sci. Discovery* **8**(1), 014003 (2015).
- ¹⁹C. S. Choi and E. Prince, "The crystal structure of cyclotrimethylene trinitramine," *Acta Crystallogr.* **B28**, 2857 (1972).
- ²⁰D. I. Millar, I. D. Oswald, D. J. Francis, W. G. Marshall, C. R. Pulham, and A. S. Cumming, "The crystal structure of β -RDX—An elusive form of an explosive revealed," *Chem. Commun.* **2009**(5), 562–564.
- ²¹W. C. McCrone, "Crystallographic data 32. RDX (cyclotrimethylenetrinitramine)," *Anal. Chem.* **22**, 956 (1950).
- ²²R. J. Karpowicz, S. T. Sergio, and T. B. Brill, " β -polymorph of hexahydro-1,3,5-trinitro-s-triazine. A Fourier transform infrared spectroscopy study of an energetic material," *Ind. Eng. Chem. Prod. Res. Dev.* **22**, 363–365 (1983).
- ²³D. I. A. Millar, "Energetic materials at extreme conditions," PhD thesis (University of Edinburgh, 2011).
- ²⁴B. J. Baer, J. Oxley, and M. Nicol, "The phase diagram of RDX (hexahydro-1,3,5-trinitro-s-triazine) under hydrostatic pressure," *High. Pressure Res.* **2**(2), 99–108 (1990).
- ²⁵A. J. Davidson, I. D. H. Oswald, D. J. Francis, A. R. Lennie, W. G. Marshall *et al.*, "Explosives under pressure the crystal structure of γ -RDX as determined by high-pressure x-ray and neutron diffraction," *CrystEngComm* **10**(2), 162–165 (2008).
- ²⁶P. J. Miller, S. Block, and G. J. Piermarini, "Effects of pressure on the thermal decomposition kinetics, chemical reactivity and phase behavior of RDX," *Combust. Flame* **83**, 174–184 (1991).
- ²⁷Z. A. Dreger and Y. M. Gupta, "Phase diagram of hexahydro-1,3,5-trinitro-1,3,5-triazine crystals at high pressures and temperatures," *J. Phys. Chem. A* **114**(31), 8099–8105 (2010).

- ²⁸M. J. Cawkwell, D. J. Luscher, F. L. Addessio, and K. J. Ramos, "Equations of state for the alpha and gamma polymorphs of cyclotrimethylene trinitramine," *J. Appl. Phys.* **119**(18), 185106 (2016).
- ²⁹J. E. Patterson, Z. A. Dreger, and Y. M. Gupta, "Shock wave-induced phase transition in RDX single crystals," *J. Phys. Chem. B* **111**(37), 10897–10904 (2007).
- ³⁰A. R. Champion, "Effect of shock compression on electrical resistivity of three polymers," *J. Appl. Phys.* **43**(5), 2216–2220 (1972).
- ³¹H. Oona, J. H. Goforth, D. G. Tasker, J. C. King, F. C. Sena, G. F. Kiuttu, and T. Cavazos, "Studies of plastic insulators under shock conditions," Technical Report, Los Alamos National Laboratory, 2001.
- ³²S. A. Sheffield, R. L. Gustavsen, and R. R. Alcon, "Porous HMX initiation studies—Sugar as an inert simulant," *AIP Conf. Proc.* **429**, 575–578 (1998).
- ³³J. T. Dickinson, M. H. Miles, W. L. Elban, and R. G. Rosemeier, "Fractoemission from cyclotrimethylenetrinitramine (RDX) explosive single crystals," *J. App. Phys.* **55**, 3994–3998 (1984).
- ³⁴M. H. Miles, J. T. Dickinson, and L. C. Jensen, "Fractoemission from single crystal pentaerythritol tetranitrate," *J. App. Phys.* **57**, 5048–5055 (1985).
- ³⁵J. T. Dickinson, L. B. Brix, and L. C. Jensen, "Electron and positive ion emission accompanying fracture of wint-o-green lifesavers and single-crystal sucrose," *J. Phys. Chem.* **88**, 1698–1701 (1984).